






**Dynamically encircling an exceptional point by microwave fields in synthetic antiferromagnets**Chaowei Sui <sup>1</sup>, Mingyu Ma,<sup>1</sup> Shaohua Yuan <sup>1</sup>, Jie Zheng <sup>1</sup>, Daqiang Gao,<sup>1</sup> Vladimir Koval <sup>2</sup>, and Chenglong Jia <sup>1,3,\*</sup><sup>1</sup>Key Laboratory for Magnetism and Magnetic Materials of the Ministry of Education, Lanzhou University, Lanzhou 730000, China<sup>2</sup>Institute of Materials Research, Slovak Academy of Sciences, Watsonova 47, 040 01 Kosice, Slovakia<sup>3</sup>Lanzhou Center for Theoretical Physics & Key Laboratory of Theoretical Physics of Gansu Province, Lanzhou University, Lanzhou 730000, China

(Received 6 September 2023; revised 28 November 2023; accepted 30 November 2023; published 18 December 2023)

The impact of dynamically encircling an exceptional point (EP) on the low-energy spin excitations in anti-parity-time (anti- $\mathcal{PT}$ ) symmetric synthetic antiferromagnets is investigated by adopting the quantum adiabatic theorem and numerical simulations. Under adiabatic conditions, the dynamic evolution of the encircling EPs is found to converge toward a low-dissipation state. When the evolution begins from a phase with broken anti- $\mathcal{PT}$  symmetry, the chiral mode switching occurs. On the other hand, a phase with preserved anti- $\mathcal{PT}$  symmetry evolves during the encircling EPs through different magnon states into the same low-dissipation final state. Despite adhering to the adiabatic conditions for evolution parameters, nonadiabatic transitions are still observed in the antiferromagnetic system and can be effectively described by changes in the dynamical and topological aspects of the final magnon state. The results, as validated using full-edged numerical micromagnetic simulations, demonstrate the ability to explore non-Hermitian state transfer in flexible magnetic systems.

DOI: [10.1103/PhysRevB.108.214420](https://doi.org/10.1103/PhysRevB.108.214420)**I. INTRODUCTION**

Over the past few decades, non-Hermitian systems exhibiting parity-time ( $\mathcal{PT}$ ) symmetry have attracted great attention due to their unique and interesting properties [1–19]. Extensive theoretical studies on non-Hermitian systems have demonstrated that the topological characteristics of an exceptional point (EP) [20,21] are usually responsible for  $\mathcal{PT}$ -symmetry-related phenomena, such as chiral mode switching during adiabatically encircling EPs [22–25]. In addition to nonreciprocal time evolution, enhanced sensitivity near EPs has been reported [26]. It was shown that, due to symmetry breaking, gain or loss can be observed when crossing the EPs. However, the requirement for passive external gain to counterbalance losses was strongly limiting in the wide use of the non-Hermitian  $\mathcal{PT}$ -symmetric systems.

Our earlier investigation of the low-energy spin dynamics (i.e., spin waves with magnons as quanta of excitations) in synthetic antiferromagnetic (SyAFM) systems, which consist of two ferromagnetic (FM) layers coupled AFM through the Ruderman-Kittel-Kasuya-Yosida (RKKY) interaction, have revealed an intrinsic anti- $\mathcal{PT}$  symmetry that circumvents the need for passive construction [26]. The anti- $\mathcal{PT}$  symmetry [27–34], considered a plausible variant of  $\mathcal{PT}$  symmetry, is often represented by the Hamiltonian  $\mathcal{H}_{APT} = \pm i\mathcal{H}_{PT}$  [35], which represents both the shared properties and distinctions. In this paper, taking advantage of the inherent properties of SyAFMs, we investigate the dynamics of quasistatic evolution around EPs in the parameter space.

Magnetic systems exchange energy with the external environment, resulting in nonunitary magnetic dynamics [36].

In such a case, the Hamiltonian governing magnons is inherently non-Hermitian and leads to complex dynamics that requires additional parameters for quantifying properties. By investigating the evolution of magnon states in SyAFM systems and considering both dynamical and topological aspects while quasistatically controlling system parameters encircling the EP using microwave fields, we demonstrate the value of adiabatic predictions in determining a lower dissipation final state. Moreover, this approach allows us to distinguish distinct dynamical processes in the non-Hermitian SyAFM system based on the evolution of different initial states and evolution directions. For topological property evaluation, we will determine whether the evolution path encircles the EP and define its encircling direction by the vorticity of the evolution. Moreover, the vorticity will be shown as an evidence of the chiral mode switching during the magnon state evolution.

Like  $\mathcal{PT}$ -symmetric systems, the evolution of magnon states in SyAFM systems is highly sensitive to the initial conditions and exhibits a chiral response at the EP. Nonadiabatic transitions (NATs) and chiral mode transfer occur during adiabatic encircling of the EP when starting from the anti- $\mathcal{PT}$ -symmetry-broken (APT<sub>B</sub>) phase, while nonchiral dynamics governs the evolution from the anti- $\mathcal{PT}$ -symmetry-preserved (APT) phase. To describe non-Hermitian state transfer qualitatively, we introduce a ratio of final magnon states between upper and lower sublattices of SyAFMs following the chiral and state evolutions in the APT<sub>B</sub> and APT phases, respectively. The occurrence of NAT processes can be identified by comparing amplitude norms of different magnon states. The amplitude norms are closely related to the trajectory of evolution, as the state evolution primarily arises due to the accumulation of kinetic phases. Micromagnetic simulations are employed to evidence the NAT and topological chiral mode transfer through dynamically

\*cljia@lzu.edu.cn

encircling the EP in SyAFMs subjected to microwave fields. The proposed approach provides a straightforward and practical method for manipulating quantum states in SyAFM systems.

## II. ANTI- $\mathcal{PT}$ SYMMETRIC SPIN DYNAMICS

For a symmetric SyAFM system composed of two identical FM layers interacting against each other, the spin dynamics can be described by the Landau-Lifshitz-Gilbert (LLG) equation [37]:

$$\partial_t \mathbf{m}_i = -\gamma \mathbf{m}_i \times [\mathbf{H}_i^{\text{eff}} + \alpha \partial_t \mathbf{m}_i], \quad (1)$$

where  $\mathbf{m}_i$  (with  $i = 1, 2$ ) denotes the magnetization of the two FM sublayers,  $\gamma$  is the gyromagnetic ratio, and  $\alpha$  is the Gilbert damping constant. The effective magnetic field acting locally on sublattice  $\mathbf{m}_i$  can be written as follows:  $\mathbf{H}_i^{\text{eff}} = A \nabla^2 \mathbf{m}_i + K_z m_i^z \hat{e}_z - J \mathbf{m}_i + H$  ( $\bar{1} = 2, \bar{2} = 1$ ) [38], where  $A$  is the Heisenberg exchange coupling constant in each  $m_i$  layer,  $K_z > 0$  is the effective uniaxial anisotropy along the easy  $z$  axis (out-of-plane direction),  $J > 0$  is the (AFM) RKKY interaction coupling coefficient, and  $H$  is the external magnetic field along the normal  $z$  direction.

To unveil the anti- $\mathcal{PT}$  symmetry of low-energy excitations, we have studied spin waves by perturbing the magnetic moments  $\mathbf{m}_i$  from their equilibrium positions,  $\mathbf{m}_i = m_i^0 \hat{e}_z + \delta \mathbf{m}_i$ , with  $|m_i^0| \approx 1$  and  $|\delta \mathbf{m}_i| \ll 1$ . In this way, the Schrödinger-like equation regarding  $\delta \mathbf{m}_i$  can be obtained as  $i \partial_t |\Psi(\mathbf{r}, t)\rangle = \mathcal{H} |\Psi(\mathbf{r}, t)\rangle$ , where  $|\Psi(\mathbf{r}, t)\rangle = [\psi_1, \psi_2]^T = [\delta m_1^x - i \delta m_1^y, \delta m_2^x - i \delta m_2^y]^T$ , and

$$\mathcal{H} = \begin{bmatrix} (E_k + H)(1 - i\alpha) & J(1 - i\alpha) \\ -J(1 + i\alpha) & -(E_k - H)(1 + i\alpha) \end{bmatrix}, \quad (2)$$

with  $E_k = A \mathbf{k}^2 + K_z + J$  in the long-wavelength limit of a plane-wave ansatz. Here,  $\mathbf{k}$  stands for the wave vector of propagating spin waves.

Now, let us consider the SyAFM with  $\mathcal{PT}$  symmetry. A parity operation  $\hat{P}$  corresponds to applying the Pauli operator  $\sigma_x$ . The time-reversal  $\hat{T}$  is defined as  $i \rightarrow -i$  and  $t \rightarrow -t$ . It is well known that the presence of an external magnetic field  $H$  breaks time-reversal symmetry. To investigate the inherent properties of SyAFM systems, we firstly consider the external magnetic field  $H = 0$ . The Hamiltonian now satisfies the anticommutator relation  $\{\mathcal{H}_0, \hat{P}\hat{T}\} = 0$ , indicating that the low-energy spin dynamics in SyAFMs is anti- $\mathcal{PT}$  symmetric.

The eigenvalues of  $\mathcal{H}_0$  are

$$\omega^\pm = i E_k (-\alpha \pm \sqrt{\xi_k^2 - 1}), \quad (3)$$

where  $\xi_k = J \sqrt{1 + \alpha^2} / E_k$ .

(i) For purely imaginary  $\omega_\pm$  when  $|\xi_k| > 1$ , the eigenvectors read

$$|\Psi_{\text{APT}}^\pm\rangle = [\text{sech } \varphi \pm i \tanh \varphi, -e^{i\eta}]^T, \quad (4)$$

where  $\tanh \varphi = \sqrt{1 - 1/\xi_k^2}$  and  $\tan \eta = \alpha$ . These states  $|\Psi_{\text{APT}}^\pm\rangle$  are also eigenvectors of the  $\hat{P}\hat{T}$  operator [39], and it is clear that the spin excitations in the two sublattices have equal amplitudes. Thus, the state  $|\Psi_{\text{APT}}^\pm\rangle$  possess anti- $\mathcal{PT}$  symmetry. This symmetry is preserved until  $\mathbf{k}$  reaches

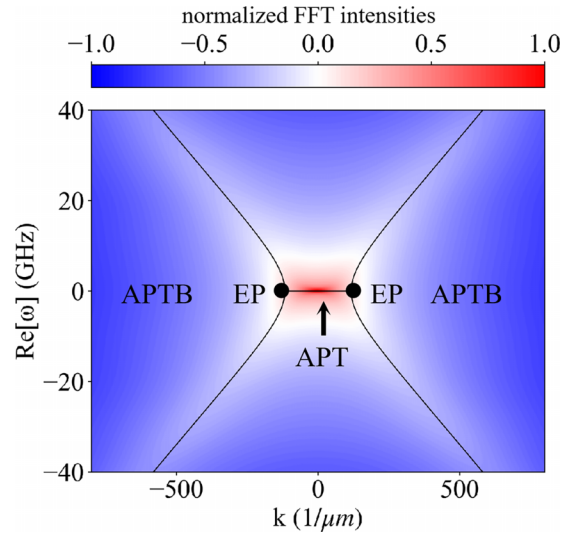


FIG. 1. The real part of the magnonic energy bands exhibits two exceptional points (EPs) along the wave vector  $k$ . The region within  $|k| < |k_{EP}|$  corresponds to the anti- $\mathcal{PT}$ -symmetry-preserved (APT) phase, while for  $|k| > |k_{EP}|$ , the anti- $\mathcal{PT}$  symmetry is broken, and the APTB phase emerges. The renormalized fast Fourier transform (FFT) intensities represent the micromagnetic simulation results with the parameters  $A = 0.4$  pJ/m,  $K_z = 0.5$  kJ/m<sup>3</sup>,  $J = 1.2$  MJ/m<sup>3</sup>, and  $\alpha = 0.1$ . The solid black lines are the analytical eigenvalues  $\omega^\pm$ .

$\mathbf{k}_{EP} = \pm[(J(\sqrt{1 + \alpha^2} - 1) - K_z)/A]^{1/2}$ , where the EP occurs at  $|\xi_k| = 1$ , leading to a breakdown of the anti- $\mathcal{PT}$  symmetry, as shown in Fig. 1.

(ii) The system enters the APTB phase with complex eigenvalues if  $|\xi_k| < 1$  with large wave vectors  $|\mathbf{k}|$ . The corresponding eigenvectors are given by the following expression [40]:

$$\begin{aligned} |\Psi_a^+\rangle &= \left[ \cosh \frac{\phi}{2}, -\sinh \frac{\phi}{2} e^{i\eta} \right]^T, \\ |\Psi_b^-\rangle &= \left[ -\sinh \frac{\phi}{2}, \cosh \frac{\phi}{2} e^{i\eta} \right]^T, \end{aligned} \quad (5)$$

where  $\tanh \phi = \xi_k$ ,  $\tan \eta = \alpha$ . Considering  $\cosh^2 \frac{\phi}{2} - \sinh^2 \frac{\phi}{2} = 1$ , one gets that  $\mathbf{m}_1$  and  $\mathbf{m}_2$  precesses with different cone angles in two adjacent FM sublayers. The left- and right-circularly polarized modes  $|\Psi_a^+\rangle$  and  $|\Psi_b^-\rangle$  are dominated by the precession in the upper and lower sublayers, resulting in a small intrinsic magnetization  $\mathbf{m} = (\mathbf{m}_1 + \mathbf{m}_2)/2$ . Thus, the emergent magnetization  $\mathbf{m}$  in collinear SyAFM systems indicates a breaking of the anti- $\mathcal{PT}$  symmetry.

Obviously, in the absence of an external magnetic field, the spin dynamics of SyAFMs possesses anti- $\mathcal{PT}$  symmetry. Two phases observed on either side of the EPs arise from a competitive effect between  $\mathcal{PT}$  symmetry and spin-rotational symmetry. Although, the introduction of an external magnetic field disrupts the inherent anti- $\mathcal{PT}$  symmetry, the magnetic field provides a controllable parameter for exploring dynamics of encircling the EPs in SyAFM.

### III. ENCIRCLING EP

Now, we encircle the EP in the SyAFM by manipulating the external magnetic field  $H$  and magnetic anisotropy  $K_z$ . Such manipulation can be experimentally realized in multiferroic heterojunctions (e.g., CoFeB/MgO [41] and Fe<sub>4</sub>N/BiFeO<sub>3</sub> [42]) via interfacial magnetoelectric coupling. We apply an appropriate microwave field to achieve dynamic control of the system. It should be noted that, alternatively, we could also select  $J$  or  $\alpha$  to substitute for  $K_z$  during encircling the EP, as the energy spectrum structure generated by  $J$  or  $\alpha$  along with  $H$  is analogous to that formed by  $K_z$  and  $H$ , thereby not influencing the dynamics of the system. For the sake of simplicity, but without loss of generality, we consider the resonant modes of SyAFM with the wave vector  $\mathbf{k} = 0$ . At  $H = 0$ , the EP is found at  $K_z^{\text{EP}} = J(\sqrt{1 + \alpha^2} - 1)$ . To dynamically encircle the EP, we introduce the following conditions:

$$K_z(t) = K_z^{\text{EP}} - \rho_1 \cos(nt), \quad H(t) = \rho_2 \sin(nt), \quad (6)$$

where  $\rho_1, \rho_2$  are the encircling radii,  $T = 2\pi/n$  is the period of encirclement, and parameter  $n$  quantifies adiabaticity. For adiabatic evolution, the condition  $T|\omega^+(t) - \omega^-(t)| \gg 1$  should be satisfied. The direction of the loop is counterclockwise (CCW) for  $n < 0$  and clockwise (CW) for  $n > 0$  [43–52]. When  $\rho_1 = \rho_2 = \rho$ , the encircling path forms a circle with the EP positioned at the center. Under this condition, the time-varying wave function of the system can be written as the superposition of two eigenstates [53–56]:

$$|\Psi(t)\rangle = c_a^+(t)|\Psi_a^+(t)\rangle + c_b^-(t)|\Psi_b^-(t)\rangle, \quad (7)$$

where  $|\Psi_{a,b}^\pm(t)\rangle = [\psi_1(t), \psi_2(t)]_{a,b}^{\pm,T}$  are the normalized instantaneous eigenstates. Due to the magnetic field, the eigenstate cannot be expressed by Eq. (5), and the generalized orthogonal normalization condition is no longer applicable [57]. However, we can make it orthogonal by defining a biorthogonal basis, where the eigenstate  $\langle \tilde{\Psi}(t) |$  satisfies the condition:  $\langle \tilde{\Psi}_{b,a}^\pm(t) | \mathcal{H}(t) = \langle \tilde{\Psi}_{b,a}^\pm(t) | E$  [43, 58–61]. The relationship between the eigenstates is given by  $\langle \tilde{\Psi}_{a,b}^\pm(t) | \Psi_{b,a}^\pm(t) \rangle = 0$ , and the amplitude of the eigenstate  $|\Psi_{a,b}^\pm(t)\rangle$  is defined as

$$c_{a,b}^\pm(t) = \frac{\langle \tilde{\Psi}_{a,b}^\pm(t) | \Psi(t) \rangle}{\langle \tilde{\Psi}_{a,b}^\pm(t) | \Psi_{a,b}^\pm(t) \rangle}. \quad (8)$$

The earlier theoretical studies have shown that, for a non-Hermitian system,  $|c_{a,b}^\pm(t)|^2$  does not represent the probability of being in state  $|\Psi_{a,b}^\pm(t)\rangle$  in the real sense [58]. However, it provides valuable information about the quantum state and, thus, its relative magnitude will be used for approximation of the occupation probability.

To understand the quasistatic evolution process in the SyAFM system, we firstly analyze the adiabatic prediction  $c_{ad}^\pm(t) \approx \exp[-i \int_0^t \omega^\pm(t) dt']$  [62] in the state evolution. Based on the quantum adiabatic theorem, it is less probable for the system to transform when the state evolution is slower and the energy gap is broader. As shown in Fig. 2, under the adiabatic condition, the expression  $|c_{ad}^+| \geq |c_{ad}^-|$  is preserved, and the entire evolution is headed toward loss [Figs. 2(b), 2(f) and 2(j)], regardless of the initial states [Figs. 2(a), 2(e) and 2(i)]. This implies that the eigenstates with less dissipative eigenval-

ues are dominant in the SyAFM. In contrast, in non-Hermitian  $\mathcal{PT}$ -symmetric systems, the eigenvalues either increase (gain) or decrease (loss) in the symmetry-broken phase, which leads to  $|c_{ad}^-(t)| \gg |c_{ad}^+(t)|$  [54, 63]. Consequently, infinitesimal nonadiabatic couplings can be exponentially amplified, leading to a predominance of gain eigenmodes. However, in non-Hermitian anti- $\mathcal{PT}$ -symmetric systems, the relative gain (less dissipative) eigenstates take the form of  $c_{ad}^+$  instead of  $c_{ad}^-$  [45]. In this case, the predominance of eigenstates is determined by the slow evolution or, more precisely, lower dissipation rate. The distinction between the eigenstate behavior of  $\mathcal{PT}$ - and anti- $\mathcal{PT}$ -symmetric systems emphasizes why adiabatic predictions cannot be universally applicable for non-Hermitian systems. However, they are valuable guidelines for understanding the dynamic state evolution.

The dynamic process of encircling the EP in the SyAFM system depends on both the initial state and the chosen encircling path. By comparing the instantaneous eigenvalues in Figs. 2(g) and 2(c), it is obvious that in the APT phase holds  $\omega^\pm(-\pi) = \omega^\pm(\pi)$ , indicating that the eigenvalues return back to their initial figures after completing a full cycle. Additionally, the dynamical encircling of the EP induces interband magnonic transitions [the dotted line in Fig. 2(g)], which implies a drastic change in energy. On the other hand, when evolving SyAFM from the APTB phase in one circle, two eigenvalues tend to exchange their positions:  $\omega^\pm(0) \rightleftharpoons \omega^\mp(2\pi)$  [64]. This behavior can be traced by evaluating the ratio of excitation amplitudes of two adjacent antiparallel FM sublayers, determined from instantaneous eigenvectors  $|\Psi_{a,b}^\pm(t)\rangle$ , while starting from different phases:

$$|\psi_1/\psi_2|_l = \beta_l, \quad (9)$$

where  $l = a, b$  represents the different states. If the SyAFM system evolves from the APT phase through one full cycle,  $\beta_l$  undergoes significant changes at  $t = \pi$ , while the magnon modes remain unchanged [Fig. 2(h)]:

$$|\Psi_{a,b}^\pm(0)\rangle_{\text{APT}} = |\Psi_{a,b}^\mp(2\pi)\rangle_{\text{APT}}. \quad (10)$$

On the other hand, when evolving from the APTB phase,  $\beta_l$  changes smoothly with time  $t$ , and the modes undergo a switching process [Fig. 2(d)], as follows:

$$|\Psi_{a,b}^\pm(-\pi)\rangle_{\text{APT}} \rightleftharpoons |\Psi_{b,a}^\mp(\pi)\rangle_{\text{APT}}, \quad (11)$$

It is worth noting that the presence of an external magnetic field  $H$  in the SyAFM system leads to symmetry breaking during the dynamic encircling of the EP, resulting in the emergence of a dynamic net magnetic moment. Therefore,  $\beta_l$  can be chosen as the parameter for variations in the SyAFM state. Furthermore, the results presented in Fig. 2(g) (EP within the evolutionary path) and Fig. 2(k) (EP outside of the evolutionary path) suggest that evolution from the APT phase may lead to identical initial and final eigenvalues. Without encircling the EP, no energy transition process is observed. Even when the evolution path approaches very close to the EP but does not encircle it, there still exists a finite energy gap between these two eigenvalues in the spectra, thereby reducing the probability of NATs. The EP exhibits intricate topological characteristics. When investigating the dynamic evolution of the SyAFM system by involving an encircled

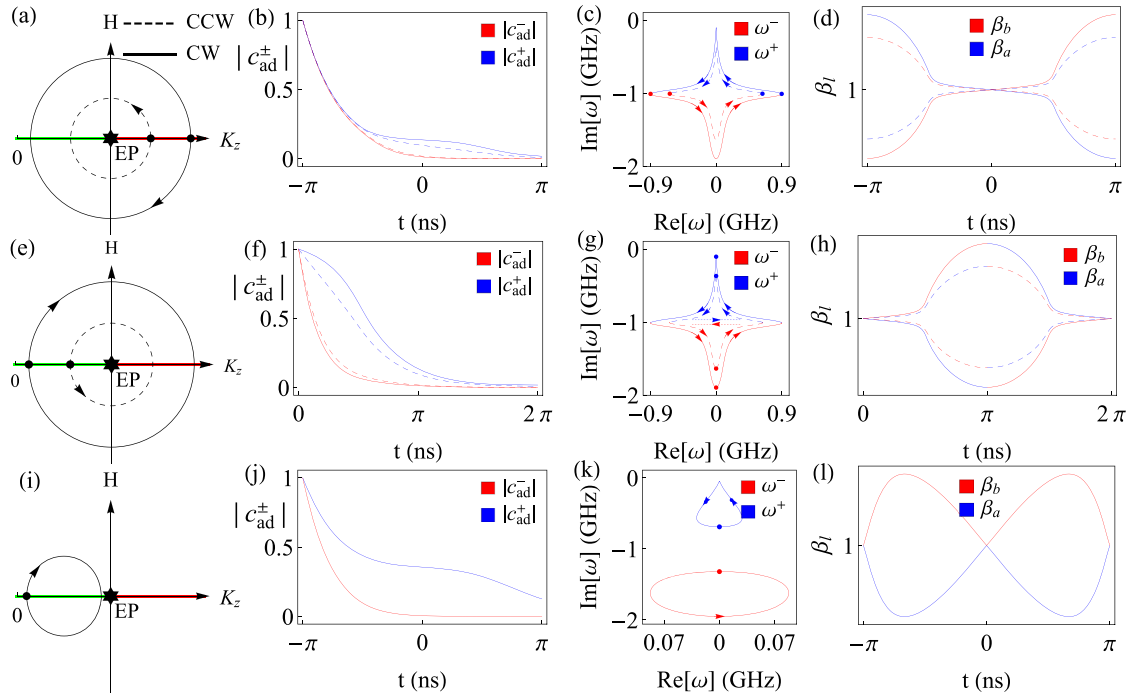


FIG. 2. Dynamic evolution of magnonic states near EP [black stars in (a), (e), and (i)]. (a)–(d) show encircling exceptional points (EPs) from the anti- $\mathcal{PT}$ -symmetry-broken (APTb) phase [red line in (a)]. (e)–(h) show encircling EPs from the anti- $\mathcal{PT}$ -symmetry-preserved (APT) phase [green line in (e)]. (i)–(l) represent nonencircling EPs from the APT phase. Encircling directions, clockwise (CW)/counterclockwise (CCW) are indicated with arrows and solid/dashed lines in (a), (e), and (i), respectively. The accumulated loss and adiabatic prediction  $|c_{ad}^{\pm}(t)|$  as well as trajectories of eigenvalues  $\omega^{\pm}(t)$  starting from different initial states (blue and red dots) are presented in (b), (f), (j), and (c), (g), and (k), respectively. Furthermore,  $\beta_l$  (with  $l = a, b$ ) in (d), (h), and (l) represent the ratio of excitation amplitudes between upper and lower ferromagnetic layers.

EP, it is insufficient to solely focus on its dynamical phase. Mailybaev *et al.* [20] have demonstrated that, in such a system, it is necessary to also examine the geometric phase. To describe topological properties of the system, a topological invariant known as the vorticity of the energy eigenvalue was introduced in calculations [65–67]. In non-Hermitian systems, for any pair of energy bands, this vorticity is defined as the winding number of energy in the complex energy plane:

$$v(\Gamma) = -\frac{1}{2\pi} \oint_{\Gamma} \nabla_t \arg[\omega^+(t) - \omega^-(t)] dt, \quad (12)$$

where  $\Gamma$  represents a closed loop in the parameter space  $\mathbf{t}$ . When the closed path  $\Gamma$  encompasses the EP,  $v(\Gamma) = \pm \frac{1}{2}$ , regardless of the evolution trajectory and time. This value physically represents one complete loop around the parameter space, but in the complex plane, it denotes a half a loop due to the degenerate EP. Only a second loop can return the system back to the initial state (except the  $\pi$  Berry phase) [68]. The  $\pm$  signs correspond to different wrapping directions, implying that the vorticity may be the cause of the antisymmetric exchange of the modes in the system with the encircled EP. If the evolution of the system no longer encompasses the EP, then the vorticity  $v(\Gamma)$  vanishes. Hence, the vorticity can be used as a criterion of the existence of an encircled EP within the evolutionary trajectory of a system.

#### IV. NAT AND CHIRAL MODE TRANSFER

To comprehensively describe the observed topological mode transfer by dynamically encircling the EP, the evolution process was numerically solved with higher precision. Figure 3 shows the dynamic process of the state evolution from the APTb phase ( $t = -\pi$ ) of the SyAFM system during the encircling of the EP. When evolving in the CW direction, both states  $|\Psi_b^- \rangle$  and  $|\Psi_a^+ \rangle$  transform into the state  $|\Psi_a^+ \rangle$  [Figs. 3(i) and 3(k)]. On the other hand, when taking a CCW trajectory, the system evolves into the state  $|\Psi_b^- \rangle$  [Figs. 3(j) and 3(l)]. The final state depends on the direction of encirclement, which indicates an asymmetric mode switching for symmetry-broken states [46,55]. When the system evolves from the APT state ( $t = 0$ ), a final state is generally independent of the evolution direction and the initial state, the system will return to the state  $|\Psi_a^+ \rangle$  after completing one loop in the parameter space [as shown in Figs. 4(i)–4(l)]. Our analysis of the final states of the SyAFM suggests that the evolution process in the system with encircled EPs favors low-dissipative states regardless of the initial state. However, it should be noted that, in SyAFM, various modes tend to dissipate due to lack of gain modes, which may hinder low-dissipation states in surpassing high-dissipation states, unless a low-dissipation state is chosen as an initial condition. From Figs. 3(a)–3(d) and 4(a)–4(d), it can be seen that the introduction of an external magnetic field  $H$  can effectively provide gain in the SyAFM system. It should be noted that a relatively



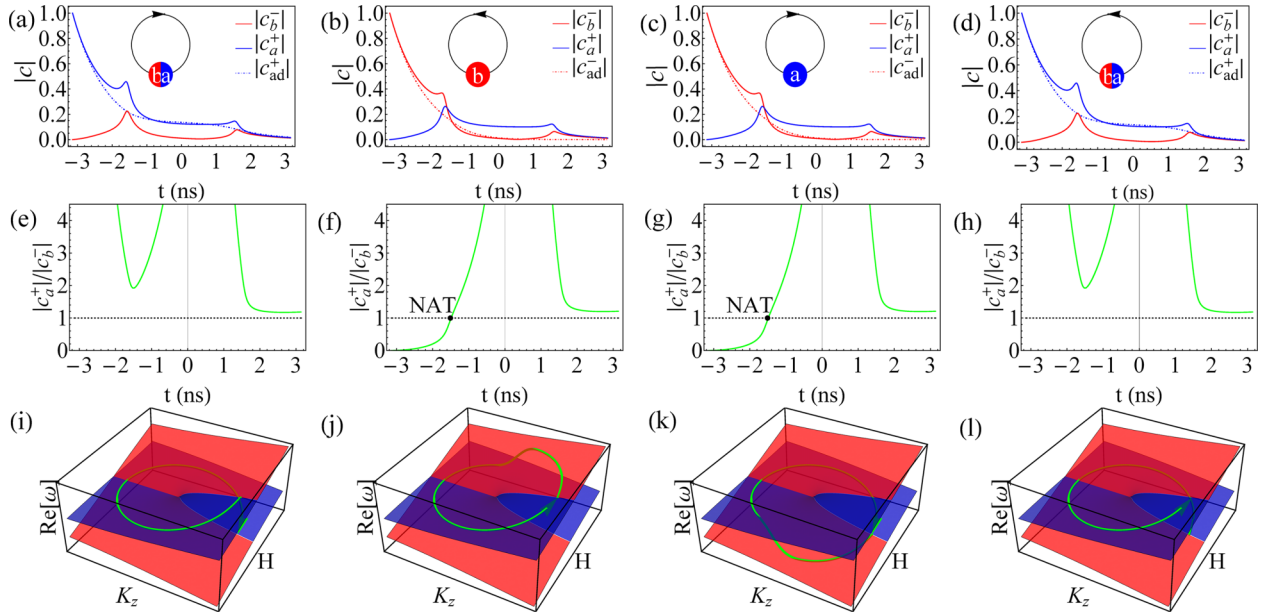


FIG. 3. Chiral mode transfer by dynamically encircling an exceptional point (EP) from an initial state in the anti- $\mathcal{PT}$ -symmetry-broken (APTb) phase. The first (last) two columns show the clockwise (CW) and counterclockwise (CCW) evolutions from the initial state  $|\Psi(-\pi)_b^- \rangle$  ( $|\Psi(-\pi)_a^+ \rangle$ ). In the first row, (a)–(d), the red solid line  $|c_b^-|$  and the blue solid line  $|c_a^+|$  represent the amplitude of instantaneous eigenstates,  $|c_{ad}^-|$  and  $|c_{ad}^+|$  are the adiabatic predictions. Nonadiabatic transition (NAT) occurs at points where the spectral lines intersect each other [(b) and (c)]. The second row, (e)–(h), shows the time-dependent ratio between two instantaneous eigenstates ( $|c_a^+|/|c_b^-|$ ), with NAT occurring at the critical points when  $|c_a^+|/|c_b^-| = 1$ . In the third row, (i)–(l), we demonstrate the encircling paths in the parameter space by the red and blue Riemann sheets, which correspond to the respective high and low dissipative states. Other parameters are  $\rho = 400 \text{ J/m}^3$ ,  $J = 0.5 \text{ MJ/m}^3$ ,  $\alpha = 0.1$ ,  $\gamma = 50.05 \text{ kHz/T}$ ,  $n = \pm 10^9 \text{ rad/s}$ , and  $M_s = 0.8 \text{ MA/m}$ .

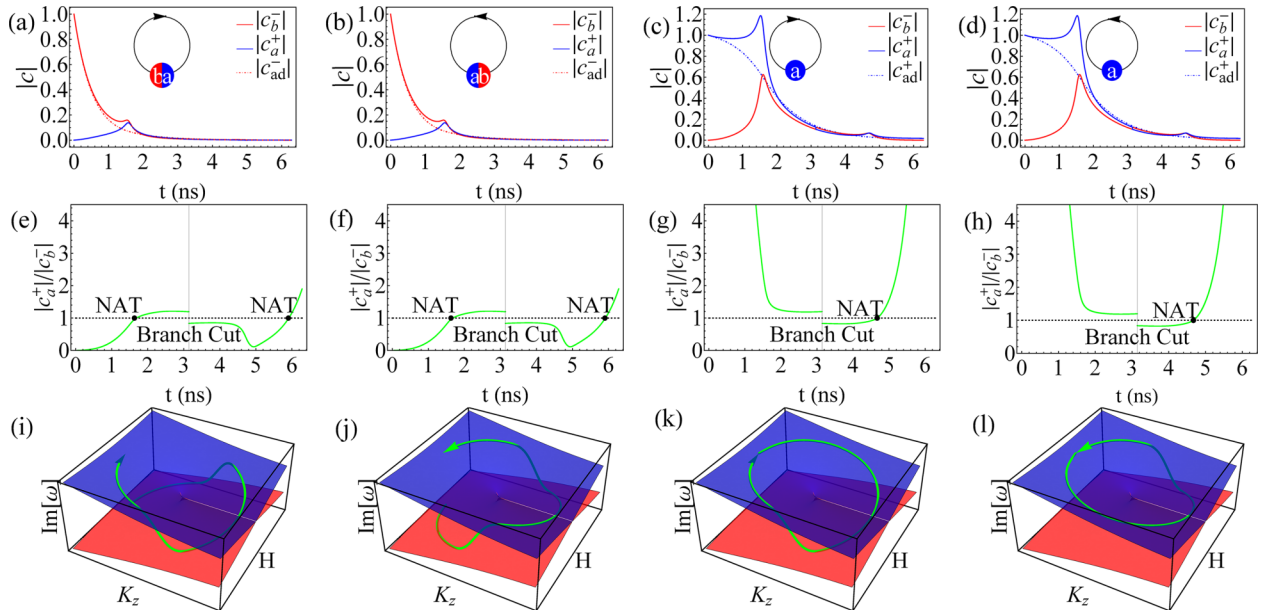


FIG. 4. Nonchiral behavior of magnonic states induced by dynamical encircling of the exceptional point (EP) in a synthetic antiferromagnet (SyAFM), the evolution from the anti- $\mathcal{PT}$ -symmetry-preserved (APT) phase. The first (last) two columns show the clockwise (CW) and counterclockwise (CCW) evolutions from the initial state  $|\Psi(0)_b^- \rangle$  ( $|\Psi(0)_a^+ \rangle$ ). In the first row, (a)–(d), the red solid line  $|c_b^-|$  and the blue solid line  $|c_a^+|$  represent the amplitude of the instantaneous eigenstates,  $|c_{ad}^-|$  and  $|c_{ad}^+|$  are the adiabatic predictions. Nonadiabatic transition (NAT) occurs at the intersection of the spectral lines [(a)–(d)]. The second row, (e)–(h), shows the time-dependent ratio between two instantaneous eigenstates ( $|c_a^+|/|c_b^-|$ ), with NAT occurring at the critical points when  $|c_a^+|/|c_b^-| = 1$ . In the third row, (i)–(l), we demonstrate the encircling paths in the parameter space by the red and blue Riemann sheets, which correspond to the respective high and low dissipative states. The other parameters are described in the caption of Fig. 3.

TABLE I. Encircling EPs from the APTB phase with different initial states and evolutionary directions.

Initial states	$ \Psi_b^-\rangle$		$ \Psi_a^+\rangle$	
	CW	CCW	CW	CCW
Final states	$ \Psi_a^+\rangle$	$ \Psi_b^-\rangle$	$ \Psi_a^+\rangle$	$ \Psi_b^-\rangle$
$\nu(\Gamma)$	-0.5	0.5	-0.5	0.5
$C_\chi$	-1.000 to 0.136 I	-0.981 to 0.134 I	-1.001 to 0.136 I	-0.982 to 0.134 I
$C_T$	1.18494	1.20858	1.20858	1.18494
NAT	0	1	1	0

large  $H$  is necessary to establish a dissipative space for the state evolutions and ensure the self-consistency of theoretical analysis.

Clearly, the adiabatic process of dynamically encircling the EP is profoundly influenced by the evolutionary trajectory. When the evolution is initiated from the red Riemann sheet of the APTB phase, a NAT is distinctly noticeable in Figs. 3(j) and 3(k). However, when the evolution trajectory starts on the blue Riemann sheets, SyAFM evolves adiabatically, as shown in Figs. 3(i) and 3(l). The adiabatic predictions, based on the results presented in Fig. 2, particularly these for  $|c_{ad}^+|$ , are consistent with the above identified evolutions. The system predominantly settles into a low-dissipation state, typically represented by the blue Riemann sheet. Similarly, due to  $|c_{ad}^+| \geq |c_{ad}^-|$ , branch cuts introduce an additional complexity into the dynamic process starting from the APT phase and heading toward a low dissipation final state of SyAFM. When the branch cuts occur, they direct the evolution states toward a highly dissipative red Riemann sheet (at  $t = \pi$ ). Such an event serves as a predecessor of at least one NAT during the evolution, as demonstrated in Figs. 4(i) and 4(j). Initially, the system transforms from a state relative to the red Riemann sheet to a state corresponding to the blue Riemann sheet. However, after encountering a branch cut, the magnon state reverts back to the red sheet. Similarly, along another trajectory [Figs. 4(k) and 4(k)], the evolution begins in the blue Riemann sheet, and just before undergoing NAT, it traverses a branch cut, shifting the system state to the red sheet. These findings are in accordance with our earlier observations that identical evolutionary trajectories invariably produce similar NAT processes.

In addition to the above-discussed evolutionary trajectory of magnon states, we have further investigated the final states to provide a more detailed description of the state evolution. For example, a considerable difference between the ratios of excitation amplitudes of the final state in the two AFM-coupled FM sublayers was observed for the system evolved

from the different (APT and APTB) phases. When the evolution starts from the APTB phase, the ratio can be expressed as

$$\psi_1(T)/\psi_2(T) = C_\chi, \quad (13)$$

where  $\chi$  represents either the CW or CCW direction. It was found that both the real and imaginary parts of  $C_\chi$  are dependent on the encircling directions (cf. Table I). Interestingly, if the APT phase is the initial phase, the ratio  $C_\chi$  is associated rather with the initial states  $|\Psi_a^+\rangle$  and  $|\Psi_b^-\rangle$  (cf. Table II). It is intricate to determine the relative eigenmode distribution with respect to final state:

$$|c_a^+(T)|/|c_b^-(T)| = C_T; \quad (14)$$

where the parameter  $C_T$  is entirely controlled by the evolutionary trajectory. This feature enabled us to utilize  $C_T$  for characterization of NATs during the adiabatic evolution. A detailed inspection of the plots in Figs. 3(a)–3(d) [and similarly Figs. 4(a)–4(d)] suggests that adiabatic predictions cannot always flawlessly anticipate  $|c_a^+|$  or  $|c_b^-|$ . A striking divergence occurs, when system time reaches either  $t = \pm\pi/2$  or  $3\pi/2$ . At these points, the system parameter approaches the EP, while  $H$  is maximized, leading to significant changes in the magnon state [Figs. 2(d) and 2(h)]. Those pronounced shifts are caused by spin-wave excitation triggered by the perturbation of the external magnetic field  $H$ . The application of the field enhances the sensitivity of the magnetic system near the EP and provides a pathway for achieving more precise measurements of the magnetic susceptibility, as reported in Ref. [69].

State evolutions in anti- $\mathcal{PT}$ -symmetric systems were found to show an opposing trend in comparison with their  $\mathcal{PT}$ -symmetric counterparts. The distinctive characteristics observed when starting the encircling EP evolution from the APTB phase in the anti- $\mathcal{PT}$ -symmetric systems can also be observed when starting the evolution from the  $\mathcal{PT}$ -symmetric phase in  $\mathcal{PT}$ -symmetric systems and vice versa. This finding

TABLE II. Encircling EPs from the APT phase with different initial states and evolutionary directions.

Initial states	$ \Psi_b^-\rangle$		$ \Psi_a^+\rangle$	
	CW	CCW	CW	CCW
Final states	$ \Psi_a^+\rangle$	$ \Psi_a^+\rangle$	$ \Psi_a^+\rangle$	$ \Psi_a^+\rangle$
$\nu(\Gamma)$	-0.5	0.5	-0.5	0.5
$C_\chi$	-0.990 to 0.071 I	-1.005 to 0.072 I	-1.001 to 0.007 I	-0.999 to 0.007 I
$C_T$	1.90167	1.90167	52.8112	52.8112
NAT	1	1	2	2

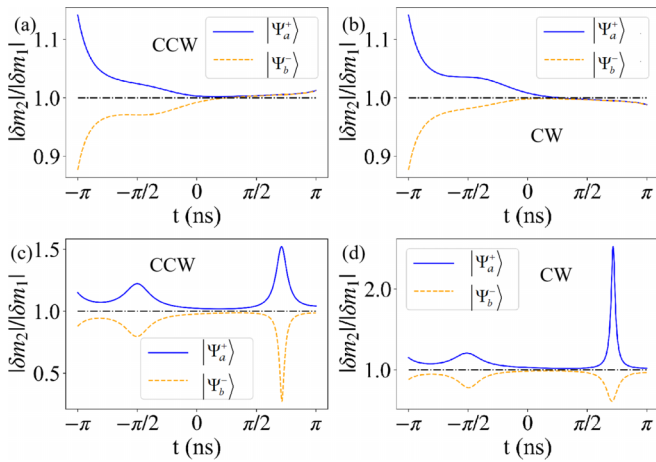


FIG. 5. Micromagnetic simulations of the dynamic evolution of synthetic antiferromagnetic (SyAFM) magnon states. (a) and (b) show the dynamic process of encircling exceptional points (EPs) from the anti- $\mathcal{PT}$ -symmetry-broken (APT $\mathcal{B}$ ) phase. (c) and (d) show the dynamic process from the APT $\mathcal{B}$  phase without encircling EP. The initial states  $|\Psi_b^- \rangle$  and  $|\Psi_a^+ \rangle$  are indicated by the orange dashed line and the blue solid line, respectively. In the simulations, the parameters are  $\rho_1 = 400$  A/m,  $\rho_2 = 300$  A/m,  $\gamma = 0.202$  MHz/T,  $\alpha = 0.1$ ,  $n = \pm 10^9$  rad/s,  $J = 10^5$  J/m $^3$ , the encircling centers of the parameters in (c) and (d) are located at  $K_z = 100998$  J/m $^3$ ,  $H = 0$  A/m.

can be extended not only to the final states of the evolution but also to a series of other characteristic parameters, including the ratio of excitation amplitudes between two adjacent FM sublayers in AFM systems [45,46,70]. From the above, one can infer that the distinctions ranging from energy band structures to evolutionary processes in non-Hermitian systems are caused by the symmetries [46,71]. Therefore, we can use the dynamical properties of the anti- $\mathcal{PT}$ -symmetric SyAFM system to predict the characteristics of the  $\mathcal{PT}$ -symmetric FM system [69]. Furthermore, we expect that the property of using the symmetry-breaking phase and the symmetry-preserving relative mixed state for filtering in the  $\mathcal{PT}$ -symmetric system can also be observed in the anti- $\mathcal{PT}$ -symmetric SyAFM system. This will provide us with additional ways for manipulating magnetic dynamics.

To further support our results, we have performed micromagnetic simulations using the OOMMF package [72]. Initially, we stimulated the SyAFM system with a microwave field  $h = \text{sinc}(2\pi ft)$  and determined the eigenfrequency  $f$  from

the fast Fourier transform analysis. Subsequently, we excited the magnon eigenmode in the APT $\mathcal{B}$  phase using the eigenfrequency  $f$  and compared the state evolution encircling and nonencircling the EP. The results of dynamically encircling the EP for the CCW and CW directions are presented in Figs. 5(a) and 5(b), respectively. From the figures, it is clear that the evolution from the APT $\mathcal{B}$  phase is chiral. On the other hand, without encircling the EP [Figs. 5(c) and 5(d)], the dynamics remains adiabatic with no chiral mode transfer. This observation is consistent with our previous analysis [Figs. 2(i)–2(l)], which showed that the large energy gap leads to adiabatic processes in the SyAFM system.

## V. CONCLUSIONS

In summary, we have investigated the chiral control and nonadiabatic transition of magnon modes in anti- $\mathcal{PT}$ -symmetric SyAFM systems by dynamically encircling an EP. Our findings demonstrate that the quantum adiabatic theorem remains a valuable tool for the description of the temporal evolution of magnon modes. The transfer of magnon modes was linked with the magnon state evolution. A chiral mode was found to occur during the evolution from the initial phase with broken anti- $\mathcal{PT}$  symmetry. When the state evolution started from the phase with preserved anti- $\mathcal{PT}$  symmetry, the final magnon state of the SyAFM system corresponded to the same final state. To distinguish the magnon states and describe the effect of the encircled EP on the state evolutions, we introduced several characteristic parameters in numerical calculations and simulations, including the vorticity ( $\nu$ ), the relative excitation amplitude ( $C_\chi$ ) in two adjacent antiparallel FM sublayers for the final mode, and the relative distribution ( $C_T$ ) of magnon eigenmodes in the final state, which effectively characterize the evolutionary trajectory of evolution. The calculated values of these parameters are summarized in Tables I and II. This paper extends our current understanding of spin waves in AFM systems and provides an approach for flexible steering and controlling quantum state.

## ACKNOWLEDGMENTS

This paper was supported by the National Natural Science Foundation of China (Grants No. 12174164, No. 91963201, and No. 11834005), the 111 Project under Grant No. B20063, the Grant Agency of the Slovak Academy of Sciences (VEGA Grant No. 2/0034/23) and the Slovak Research and Development Agency (Grant No. APVV-20-0072).

[1] C. M. Bender and S. Boettcher, Real spectra in non-Hermitian Hamiltonians having  $\mathcal{PT}$  symmetry, *Phys. Rev. Lett.* **80**, 5243 (1998).  
 [2] C. M. Bender, Introduction to  $\mathcal{PT}$ -symmetric quantum theory, *Contemp. Phys.* **46**, 277 (2005).  
 [3] C. M. Bender, S. Boettcher, and P. N. Meisinger,  $\mathcal{PT}$ -symmetric quantum mechanics, *J. Math. Phys.* **40**, 2201 (1999).  
 [4] C. M. Bender, M. V. Berry, and A. Mandilara, Generalized  $\mathcal{PT}$  symmetry and real spectra, *J. Phys. A: Math. Gen.* **35**, L467 (2002).

[5] A. Guo, G. J. Salamo, D. Duchesne, R. Morandotti, M. Volatier-Ravat, V. Aimez, G. A. Siviloglou, and D. N. Christodoulides, Observation of  $\mathcal{PT}$ -symmetry breaking in complex optical potentials, *Phys. Rev. Lett.* **103**, 093902 (2009).  
 [6] C. E. Rüter, K. G. Makris, R. El-Ganainy, D. N. Christodoulides, M. Segev, and D. Kip, Observation of parity-time symmetry in optics, *Nat. Phys.* **6**, 192 (2010).  
 [7] Y. C. Hu and T. L. Hughes, Absence of topological insulator phases in non-Hermitian  $\mathcal{PT}$ -symmetric Hamiltonians, *Phys. Rev. B* **84**, 153101 (2011).

- [8] A. Regensburger, C. Bersch, M. A. Miri, G. Onishchukov, D. N. Christodoulides, and U. Peschel, Parity-time synthetic photonic lattices, *Nature (London)* **488**, 167 (2012).
- [9] M. Brandstetter, M. Lierzter, C. Deutsch, P. Klang, J. Schoberl, H. E. Türeci, G. Strasser, K. Unterrainer, and S. Rotter, Reversing the pump dependence of a laser at an exceptional point, *Nat. Commun.* **5**, 4034 (2014).
- [10] B. Peng, Ş. K. Özdemir, F. Lei, F. Monifi, M. Gianfreda, G. L. Long, S. Fan, F. Nori, C. M. Bender, and L. Yang, Parity-time-symmetric whispering-gallery microcavities, *Nat. Phys.* **10**, 394 (2014).
- [11] J. M. Lee, T. Kottos, and B. Shapiro, Macroscopic magnetic structures with balanced gain and loss, *Phys. Rev. B* **91**, 094416 (2015).
- [12] A. Galda and V. M. Vinokur, Parity-time symmetry breaking in magnetic systems, *Phys. Rev. B* **94**, 020408(R) (2016).
- [13] K. V. Kepesidis, T. J. Milburn, J. Huber, K. G. Makris, S. Rotter, and P. Rabl,  $\mathcal{PT}$ -symmetry breaking in the steady state of microscopic gain-loss systems, *New J. Phys.* **18**, 095003 (2016).
- [14] V. V. Konotop, J. Yang, and D. A. Zezyulin, Nonlinear waves in  $\mathcal{PT}$ -symmetric systems, *Rev. Mod. Phys.* **88**, 035002 (2016).
- [15] F. Monticone, C. A. Valagiannopoulos, and A. Alù, Parity-time symmetric nonlocal metasurfaces: All-angle negative refraction and volumetric imaging, *Phys. Rev. X* **6**, 041018 (2016).
- [16] Y. Ashida, S. Furukawa, and M. Ueda, Parity-time-symmetric quantum critical phenomena, *Nat. Commun.* **8**, 15791 (2017).
- [17] R. El-Ganainy, K. G. Makris, M. Khajavikhan, Z. H. Musslimani, S. Rotter, and D. N. Christodoulides, Non-Hermitian physics and  $\mathcal{PT}$  symmetry, *Nat. Phys.* **14**, 11 (2018).
- [18] F. Quijandría, U. Naether, S. K. Özdemir, F. Nori, and D. Zueco,  $\mathcal{PT}$ -symmetric circuit QED, *Phys. Rev. A* **97**, 053846 (2018).
- [19] I. Katsantonis, S. Droulias, C. M. Soukoulis, E. N. Economou, and M. Kafesaki,  $\mathcal{PT}$ -symmetric chiral metamaterials: Asymmetric effects and  $\mathcal{PT}$ -phase control, *Phys. Rev. B* **101**, 214109 (2020).
- [20] A. A. Mailybaev, O. N. Kirillov, and A. P. Seyranian, Geometric phase around exceptional points, *Phys. Rev. A* **72**, 014104 (2005).
- [21] S.-Y. Lee, J.-W. Ryu, S. W. Kim, and Y. Chung, Geometric phase around multiple exceptional points, *Phys. Rev. A* **85**, 064103 (2012).
- [22] C. Dembowski, H.-D. Gräf, H. L. Harney, A. Heine, W. D. Heiss, H. Rehfeld, and A. Richter, Experimental observation of the topological structure of exceptional points, *Phys. Rev. Lett.* **86**, 787 (2001).
- [23] Z. Ren, D. Liu, E. Zhao, C. He, K. K. Pak, J. Li, and G.-B. Jo, Chiral control of quantum states in non-Hermitian spin-orbit-coupled fermions, *Nat. Phys.* **18**, 385 (2022).
- [24] A. Li, J. Dong, J. Wang, Z. Cheng, J. S. Ho, D. Zhang, J. Wen, X. L. Zhang, C. T. Chan, A. Alu *et al.*, Hamiltonian hopping for efficient chiral mode switching in encircling exceptional points, *Phys. Rev. Lett.* **125**, 187403 (2020).
- [25] X.-L. Zhang and C. T. Chan, Dynamically encircling exceptional points in a three-mode waveguide system, *Commun. Phys.* **2**, 63 (2019).
- [26] C. Sui, S. Yuan, X. Wang, J. Berakdar, and C. Jia, Emergent magnonic singularities in anti parity-time symmetric synthetic antiferromagnets, *New J. Phys.* **24**, 023031 (2022).
- [27] L. Ge and H. E. Türeci, Antisymmetric  $\mathcal{PT}$ -photonic structures with balanced positive- and negative-index materials, *Phys. Rev. A* **88**, 053810 (2013).
- [28] P. Peng, W. Cao, C. Shen, W. Qu, J. Wen, L. Jiang, and Y. Xiao, Anti-parity-time symmetry with flying atoms, *Nat. Phys.* **12**, 1139 (2016).
- [29] D. A. Antonosyan, A. S. Solntsev, and A. A. Sukhorukov, Parity-time anti-symmetric parametric amplifier, *Opt. Lett.* **40**, 4575 (2015).
- [30] F. Yang, Y.-C. Liu, and L. You, Anti- $\mathcal{PT}$  symmetry in dissipatively coupled optical systems, *Phys. Rev. A* **96**, 053845 (2017).
- [31] L. Jin, Scattering properties of a parity-time-antisymmetric non-Hermitian system, *Phys. Rev. A* **98**, 022117 (2018).
- [32] F. Zhang, Y. Feng, X. Chen, L. Ge, and W. Wan, Synthetic anti- $\mathcal{PT}$  symmetry in a single microcavity, *Phys. Rev. Lett.* **124**, 053901 (2020).
- [33] J. Zhao, Y. Liu, L. Wu, C.-K. Duan, Y.-x. Liu, and J. Du, Observation of anti- $\mathcal{PT}$ -symmetry phase transition in the magnon-cavity-magnon coupled system, *Phys. Rev. Appl.* **13**, 014053 (2020).
- [34] X.-g. Wang, D. Schulz, G.-h. Guo, and J. Berakdar, Magnon dynamics in parity-time-symmetric dipolarly coupled waveguides and magnonic crystals, *Phys. Rev. Appl.* **18**, 024080 (2022).
- [35] Y. Choi, C. Hahn, J. W. Yoon, and S. H. Song, Observation of an anti- $\mathcal{PT}$ -symmetric exceptional point and energy-difference conserving dynamics in electrical circuit resonators, *Nat. Commun.* **9**, 2182 (2018).
- [36] M. C. Hickey and J. S. Moodera, Origin of intrinsic Gilbert damping, *Phys. Rev. Lett.* **102**, 137601 (2009).
- [37] C. Kittel, Theory of antiferromagnetic resonance, *Phys. Rev.* **82**, 565 (1951).
- [38] J. Lan, W. Yu, and J. Xiao, Antiferromagnetic domain wall as spin wave polarizer and retarder, *Nat. Commun.* **8**, 178 (2017).
- [39] M. Maamache and L. Kheniche, Anti- $\mathcal{PT}$  symmetry for a non-Hermitian Hamiltonian, *Prog. Theor. Exp. Phys.* **2020**, 123A01 (2020).
- [40] C. Jia, M. Chen, A. F. Schäffer, and J. Berakdar, Chiral logic computing with twisted antiferromagnetic magnon modes, *npj Comput. Mater.* **7**, 101 (2021).
- [41] A. Deka, B. Rana, R. Anami, K. Miura, H. Takahashi, Y. C. Otani, and Y. Fukuma, Electric-field control of interfacial in-plane magnetic anisotropy in CoFeB/MgO junctions, *Phys. Rev. B* **101**, 174405 (2020).
- [42] L. Yin, X. Wang, and W. Mi, Electric-field tunable perpendicular magnetic anisotropy in tetragonal Fe<sub>4</sub>N/BiFeO<sub>3</sub> heterostructures, *Appl. Phys. Lett.* **111**, 032404 (2017).
- [43] M. V. Berry and R. Uzdin, Slow non-Hermitian cycling: Exact solutions and the Stokes phenomenon, *J. Phys. A: Math. Theor.* **44**, 435303 (2011).
- [44] T. J. Milburn, J. Doppler, C. A. Holmes, S. Portolan, S. Rotter, and P. Rabl, General description of quasiadiabatic dynamical phenomena near exceptional points, *Phys. Rev. A* **92**, 052124 (2015).
- [45] A. U. Hassan, B. Zhen, M. Soljacic, M. Khajavikhan, and D. N. Christodoulides, Dynamically encircling exceptional points: Exact evolution and polarization state conversion, *Phys. Rev. Lett.* **118**, 093002 (2017).
- [46] X. L. Zhang, T. Jiang, and C. T. Chan, Dynamically encircling an exceptional point in anti-parity-time symmetric



- systems: Asymmetric mode switching for symmetry-broken modes, *Light Sci. Appl.* **8**, 88 (2019).
- [47] W. Liu, Y. Wu, C. K. Duan, X. Rong, and J. Du, Dynamically encircling an exceptional point in a real quantum system, *Phys. Rev. Lett.* **126**, 170506 (2021).
- [48] T. E. Lee, Anomalous edge state in a non-Hermitian lattice, *Phys. Rev. Lett.* **116**, 133903 (2016).
- [49] H. Menke, M. Klett, H. Cartarius, J. Main, and G. Wunner, State flip at exceptional points in atomic spectra, *Phys. Rev. A* **93**, 013401 (2016).
- [50] X.-L. Zhang and C. T. Chan, Hybrid exceptional point and its dynamical encircling in a two-state system, *Phys. Rev. A* **98**, 033810 (2018).
- [51] A. Galda and V. M. Vinokur, Exceptional points in classical spin dynamics, *Sci. Rep.* **9**, 17484 (2019).
- [52] L. Geng, W. Zhang, X. Zhang, and X. Zhou, Topological mode switching in modulated structures with dynamic encircling of an exceptional point, *Proc. Math. Phys. Eng. Sci.* **477**, 20200766 (2021).
- [53] D. Long, X. Mao, G.-Q. Qin, H. Zhang, M. Wang, G.-Q. Li, and G.-L. Long, Dynamical encircling of the exceptional point in a largely detuned multimode optomechanical system, *Phys. Rev. A* **106**, 053515 (2022).
- [54] R. Uzdin, A. Mailybaev, and N. Moiseyev, On the observability and asymmetry of adiabatic state flips generated by exceptional points, *J. Phys. A: Math. Theor.* **44**, 435302 (2011).
- [55] J. Doppler, A. A. Mailybaev, J. Böhm, U. Kuhl, A. Girschik, F. Libisch, T. J. Milburn, P. Rabl, N. Moiseyev, and S. Rotter, Dynamically encircling an exceptional point for asymmetric mode switching, *Nature (London)* **537**, 76 (2016).
- [56] X.-L. Zhang, S. Wang, B. Hou, and C. T. Chan, Dynamically encircling exceptional points: *In situ* control of encircling loops and the role of the starting point, *Phys. Rev. X* **8**, 021066 (2018).
- [57] C. Jia, D. Ma, A. F. Schäffer, and J. Berakdar, Twisted magnon beams carrying orbital angular momentum, *Nat. Commun.* **10**, 2077 (2019).
- [58] S. Ibáñez and J. G. Muga, Adiabaticity condition for non-Hermitian Hamiltonians, *Phys. Rev. A* **89**, 033403 (2014).
- [59] Q. Z. Lv, H. Bauke, Q. Su, C. H. Keitel, and R. Grobe, Bosonic pair creation and the Schiff-Snyder-Weinberg effect, *Phys. Rev. A* **93**, 012119 (2016).
- [60] C. Dembowski, B. Dietz, H. D. Graf, H. L. Harney, A. Heine, W. D. Heiss, and A. Richter, Encircling an exceptional point, *Phys. Rev. E* **69**, 056216 (2004).
- [61] W. Tang, X. Jiang, K. Ding, Y.-X. Xiao, Z.-Q. Zhang, C. T. Chan, and G. Ma, Exceptional nexus with a hybrid topological invariant, *Science* **370**, 1077 (2020).
- [62] G. Dridi, S. Guérin, H. R. Jauslin, D. Viennot, and G. Jolicard, Adiabatic approximation for quantum dissipative systems: Formulation, topology, and superadiabatic tracking, *Phys. Rev. A* **82**, 022109 (2010).
- [63] Y. Choi, C. Hahn, J. W. Yoon, S. H. Song, and P. Berini, Extremely broadband, on-chip optical nonreciprocity enabled by mimicking nonlinear anti-adiabatic quantum jumps near exceptional points, *Nat. Commun.* **8**, 14154 (2017).
- [64] N. Moiseyev, *Non-Hermitian Quantum Mechanics*, 1st ed. (Cambridge University Press, Cambridge, 2011).
- [65] H. Shen, B. Zhen, and L. Fu, Topological band theory for non-Hermitian Hamiltonians, *Phys. Rev. Lett.* **120**, 146402 (2018).
- [66] Z. Gong, Y. Ashida, K. Kawabata, K. Takasan, S. Higashikawa, and M. Ueda, Topological phases of non-Hermitian systems, *Phys. Rev. X* **8**, 031079 (2018).
- [67] E. J. Bergholtz, J. C. Budich, and F. K. Kunst, Exceptional topology of non-Hermitian systems, *Rev. Mod. Phys.* **93**, 015005 (2021).
- [68] Ş. K. Özdemir, S. Rotter, F. Nori, and L. Yang, Parity-time symmetry and exceptional points in photonics, *Nat. Mater.* **18**, 783 (2019).
- [69] X. G. Wang, G. H. Guo, and J. Berakdar, Steering magnonic dynamics and permeability at exceptional points in a parity-time symmetric waveguide, *Nat. Commun.* **11**, 5663 (2020).
- [70] X.-L. Zhang, J.-F. Song, C. T. Chan, and H.-B. Sun, Distinct outcomes by dynamically encircling an exceptional point along homotopic loops, *Phys. Rev. A* **99**, 063831 (2019).
- [71] J. W. Yoon, Y. Choi, C. Hahn, G. Kim, S. H. Song, K. Y. Yang, J. Y. Lee, Y. Kim, C. S. Lee, J. K. Shin *et al.*, Time-asymmetric loop around an exceptional point over the full optical communications band, *Nature (London)* **562**, 86 (2018).
- [72] M. J. Donahue and D. G. Porter, OOMMF User's Guide, Version 1.0., *Interagency Report NISTIR 6376* (National Institute of Standards and Technology, Gaithersburg, 1999).